Journal of Drug Targeting, 2000, Vol. 8, No. 1, pp. 13–27
Reprints available directly from the publisher
Photocopying permitted by license only

Structure and Structure–Function Studies of Lipid/Plasmid DNA Complexes

ALISON J. LIN[a], N.L. SLACK[a], A. AHMAD[a], I. KOLTOVER[a], C.X. GEORGE[b], C.E. SAMUEL[b] and C.R. SAFINYA[a,*]

[a]*Department of Materials, Department of Physics,* [b]*Molecular, Cellular, and Developmental Biology Department, and Biochemistry and Molecular Biology Program, University of California, Santa Barbara, CA 93106, USA*

(Received 4 August 1999; Revised 27 October 1999; In final form 5 November 1999)

Recent synchrotron-based X-ray diffraction studies have enabled us to comprehensively solve the self-assembled structures in mixtures of cationic liposomes (CLs) complexed with linear λ-DNA. In one case the CL–DNA complexes were found to consist of a higher ordered multilamellar structure (labeled L_α^C with DNA sandwiched between cationic bilayer membranes. The membrane charge density is found to control the DNA interaxial spacing with high densities leading to high DNA compaction between lipid bilayers. A second self-assembled structure (labeled H_{II}^C) consists of linear DNA strands coated by cationic lipid monolayers and arranged on a 2D hexagonal lattice. In this paper we report on a combined X-ray diffraction and optical microscopy study of CLs complexed with functional supercoiled plasmid DNA. We describe the self-assembled structures in cell culture medium for both a high transfectant complex (DOTAP/DOPE, $\Phi_{DOPE} = 0.72$) and a low transfectant complex (DOTAP/DOPC, $\Phi_{DOPC} = 0.72$). Fluorescence optica microscopy shows two distinct interactions between these two types of complexes and mouse fibroblast L-cells, demonstrating the existence of a correlation between structure and transfection efficiency.

Keywords: Nonviral gene delivery, Self-assembled structures, Cationic lipid, X-ray diffraction, Optical microscopy

1. INTRODUCTION

Gene therapy depends on the successful transfer and expression of extracellular DNA to mammalian cells, with the aim of replacing a defective or adding a missing gene (Friedmann, 1997; Felgner, 1997; Miller, 1998; Crystal, 1995; Zhu *et al.*, 1993; Nabel *et al.*, 1993; Mulligan, 1993). At present, viral-based vectors (retroviruses, adenoviruses, adeno-associated viruses) are the most common gene carriers used by researchers developing gene delivery systems because of their high efficiency of transfer and expression (Friedmann, 1997; Crystal, 1995; Mulligan, 1993). Each viral-based vector has

* Corresponding author. Tel.: +(805)893 8635. Fax: +(805)893 7221. E-mail: safinya@mrl.ucsb.edu.

advantages and disadvantages and it will be many years before the optimal vector is designed.

There has been much recent activity in the development of synthetic nonviral delivery systems (Friedmann, 1997; Felgner and Rhodes, 1991; Felgner, 1997; Miller, 1998; Zhu *et al.*, 1993; Nabel *et al.*, 1993; Behr, 1994; Remy *et al.*, 1994; Singhal and Huang, 1994; Lasic and Templeton, 1996; Marshall, 1995). The conventional nonviral transfer methodologies, which have transfection rates significantly lower than viral transfection rates, include anionic liposomes which encapsulate nucleic acid, calcium-phosphate precipitation, and use of polycationic reagents (DEAE-dextran or polylysine). Some of the advantages of using nonviral vectors for gene delivery include the fact that plasmid DNA constructs used in deliveries are more readily prepared than viral constructs, they have no viral genes to cause disease, and they are nonimmunogenic due to a lack of proteins.

The entire field of gene therapy based on synthetic nonviral delivery systems has undergone a renaissance since the initial paper by Felgner *et al.* (1987) which was soon followed by numerous other groups demonstrating *in vivo* gene expression in targeted organs (Zhu *et al.*, 1993) and in human clinical trials (Nabel *et al.*, 1993). Felgner *et al.* discovered that cationic liposomes (CLs) (closed bilayer membrane shells of lipid molecules) when mixed with DNA to form CL–DNA complexes with an overall positive charge enhance transfection (i.e. the transfer of plasmid into cells followed by expression). They hypothesized that the enhancement of transfection efficiency was due to a more effective adsorption of CL–DNA complexes to the anionic plasma membrane of mammalian cells via electrostatic interactions. Compared to other nonviral delivery systems, CLs tend to mediate a higher level of transfection in a majority of cell lines studied to date (Lasic and Templeton, 1996). Using CLs, gene expression of chloramphenicol acetyltransferase (CAT) activity has been found in mice lungs and brain (Brigham *et al.*, 1989; Hazinski *et al.*, 1991; Ono *et al.*, 1990) and in brain tissue of frog embryos (Malone, 1989; Holt *et al.*, 1990). *In vivo* CAT expression of aerosol administered plasmid DNA (pCIS–CAT) complexed with CLs in mouse lung has also been demonstrated (Stribling *et al.*, 1992).

Current viral vectors have a maximum gene carrying capacity of 40 kbp (Friedmann, 1997; Crystal, 1995). Without doubt, one of the principle and most exciting advantages of nonviral over viral methods for gene delivery is the potential of transferring and expressing (transfecting) large pieces of DNA in cells. The feasibility was clearly demonstrated when partial sections of first-generation human artificial chromosomes (HACs) of order 1 Mbp were transferred into cells using CLs, although extremely inefficiently (Harrington *et al.*, 1997; Roush, 1997). The future development of HAC vectors will be extremely important for gene therapy applications; because of their very large size capacity, HACs will have the ability of delivering not only entire human genes (in many cases exceeding 100 kbp) but also their regulatory sequences, which are needed for the spatial and temporal regulation of expression.

While the transfection rates and reproducibility in many cells have been found to be enhanced using CL–DNA complexes compared to other more traditional nonviral delivery systems, the mechanism of transfection via CLs remains largely unknown (Friedmann, 1997; Felgner and Rhodes, 1991; Felgner, 1997; Miller, 1998; Crystal, 1995; Zhu *et al.*, 1993; Nabel *et al.*, 1993; Mulligan, 1993; Behr, 1994; Remy *et al.*, 1994; Singhal and Huang, 1994; Lasic and Templeton, 1996). At present, hundreds of plasmid DNA molecules are required for successful gene transfer and expression. The low transfection efficiencies with nonviral methods result from a general lack of knowledge regarding (i) the structures of CL–DNA complexes and (ii) their interactions with cell membranes and the events leading to release of DNA in the cytoplasm for delivery to the nucleus. It is only recently that we are beginning to understand the self-assembled structures of CL–DNA complexes in different lipid–membrane systems (Raedler *et al.*, 1997; 1998; Salditt *et al.*, 1997; 1998; Lasic *et al.*, 1997; Pitard *et al.*, 1997; Safinya *et al.*, 1998; Safinya and Koltover, 1999; Koltover *et al.*, 1998; 1999). In this paper, we present our

experimental findings correlating transfection efficiencies, structures of complexes containing functional supercoiled DNA, and pathways of DNA entry into cells. We expect that the transfection efficiencies of nonviral delivery methods may be improved through insights into transfection-related mechanisms at the molecular and self-assembled levels.

2. BACKGROUND

Felgner *et al.* (1987) (Felgner and Rhodes, 1991) originally proposed a "bead-on-string" structure of the CL–DNA complexes and pictured the DNA strand decorated with distinctly attached liposomes. Electron microscopy (EM) studies have reported on a variety of structures including string-like structures and indications of fusion of liposomes in metal-shadowing EM (Gershon *et al.*, 1993), oligolamellar structures in cryo-transmission EM (Gustafsson *et al.*, 1995), and tubelike images possibly depicting lipid bilayer covered DNA observed in freeze-fracture EM (Sternberg *et al.*, 1994).

We have previously carried out a combined *in situ* optical microscopy and X-ray diffraction (XRD) study of CL–DNA complexes (Raedler *et al.*, 1997) where the CLs consisted of mixtures of neutral (so called "helper-lipid") DOPC (di-oleoyl phosphatidyl choline) and cationic DOTAP (di-oleoyl trimethylammonium propane). High resolution small angle XRD has revealed that the structure is different from the hypothesized "bead-on-string" structure (Felgner *et al.*, 1987; Felgner and Rhodes, 1991). The addition of linear lambda-phage DNA (48 kbp) to binary mixtures of CLs (mean diameter of 70 nm) induces a topological transition from liposomes into collapsed condensates in the form of optically birefringent liquid crystalline globules with size on the order of 1 μm.

We show in Fig. 1A differential-interference-contrast (DIC) optical images of CL–DNA complexes for four lipid (L) to λ-DNA (D) weight ratios (L = DOTAP + DOPC, 1 : 1). Similar images are observed when λ-DNA is replaced by supercoiled plasmid DNA (unpublished data). At low DNA concentrations (Fig. 1A, $L/D \approx 50$), in contrast to the pure liposome solution where no objects > 0.2 μm are seen, 1 μm large globules are observed. The globules coexist with excess liposomes. As more DNA is added, the globular condensates form larger chain-like structures (Fig. 1A, $L/D \approx 10$).

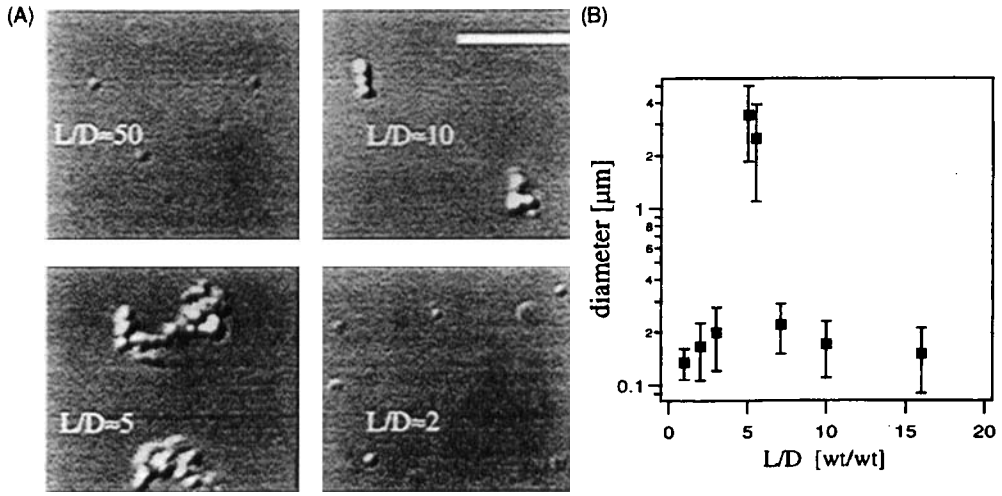

FIGURE 1 (A) High resolution DIC optical images of CL–DNA complexes forming distinct condensed globules in mixtures of different lipid to DNA weight ratio (L/D). L/D = 4.4 is the isoelectric point, CL–DNA complexes are positively charged for L/D = 50 and 10, and negatively charged for L/D = 2. The positive (negative) regime contains excess lipid (DNA). Bar is 10 μm. (B) Average size of the lipid–DNA complexes measured by dynamic light scattering. (Adapted from Raedler *et al.*, 1997).

At L/D ≈ 5, the chain-like structures flocculate into large aggregates of distinct globules. For L/D < 5, the complex size is smaller and stable in time again (Fig. 1A, L/D ≈ 2) and coexists with excess DNA. Fluorescence microscopy of the DNA (labeled with YOYO) and the lipid (labeled with Texas Red-DHPE) shows that the individual globules contain both lipid and DNA. Polarized microscopy shows that the distinct globules are birefringent indicative of their liquid crystalline nature (Koltover *et al.*, 1998).

The size dependence of the complexes as a function of L/D (Fig. 1B) is independently measured by dynamic light scattering. The large error bars represent the broad polydispersity of the system. The size dependence of the aggregates can be understood in terms of a charge-stabilized colloidal suspension. The charge of the complexes is measured by their electrophoretic mobility in an external electric field (Raedler *et al.*, 1997). For L/D > 5 (Fig. 1A; L/D ≈ 50 or 10), the complexes are positively charged, while for L/D < 5 (Fig. 1A; L/D ≈ 2), the complexes are negatively charged. The charge reversal is in good agreement with the stoichiometrically expected charge balance of the components DOTAP and DNA at L/D ≈ 4.4 (wt./wt.) where L = DOTAP + DOPC in equal weights. Thus, the positively and negatively charged complexes, at L/D ≈ 50 and 2, respectively, repel each other and remain separate and small, while as L/D approaches 5, the nearly neutral complexes collide and tend to stick due to van der Waals attraction creating large aggregates.

The small-angle-X-ray scattering (SAXS) experiments (Raedler *et al.*, 1997) reveal a novel self-assembled structure for the condensed globules consisting of mixtures of CLs and DNA. Figure 2 is a plot of SAXS data of λ-DNA–DOPC/DOTAP complexes as a function of increasing Φ_{DOPC} (the weight fraction of DOPC in the DOPC/DOTAP CL mixtures). The data is consistent with a complete topological rearrangement of liposomes and DNA into a multilayer structure with DNA intercalated between the bilayers (Fig. 3, denoted L_α^C). To see this, we first consider complexes of DNA and

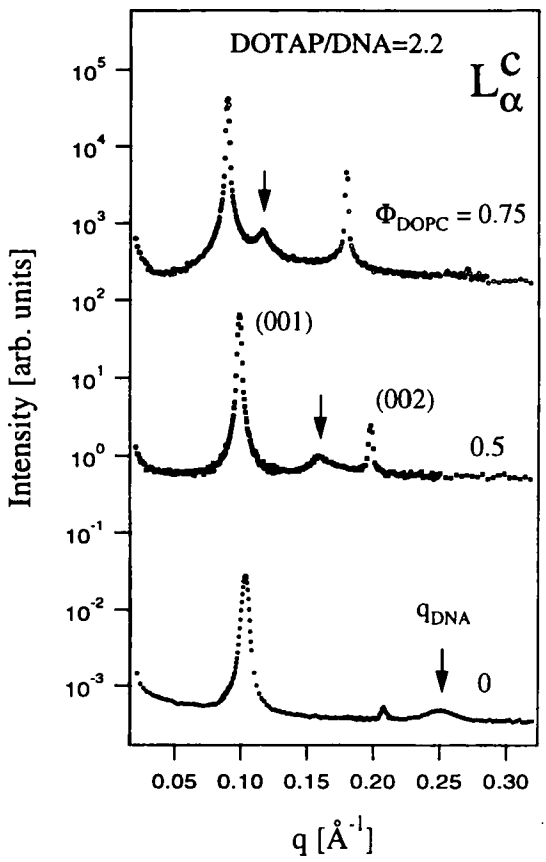

FIGURE 2 SAXS scans of CL–DNA complexes at constant DOTAP/DNA = 2.2 (near the isoelectric point) with increasing DOPC/DOTAP which shows the DNA peak (arrow) moving towards smaller q as L/D (and Φ_{DOPC}) increases. L = DOTAP + DOPC, D = DNA. (Adapted from Raedler *et al.*, 1997; Salditt *et al.*, 1997; Koltover *et al.*, 1999).

DOTAP at $\Phi_{DOPC} = 0$ (Fig. 2, bottom). The two sharp peaks at $q = 0.11$ and 0.22 Å^{-1} correspond to the (00L) peaks of a layered structure with an interlayer spacing $d(= \delta_m + \delta_w) = 57$ Å. The membrane thickness and water gap are denoted by δ_m and δ_w, respectively (Fig. 3).

In the absence of DNA, membranes of the cationic lipid DOTAP exhibit strong long-range interlayer electrostatic repulsions that overwhelm the van der Waals attraction (Roux and Safinya, 1988; Safinya, 1989). In this case, as the volume fraction Φ_w of water is increased, the L_α phase swells and the intermembrane distance d (which is measured by

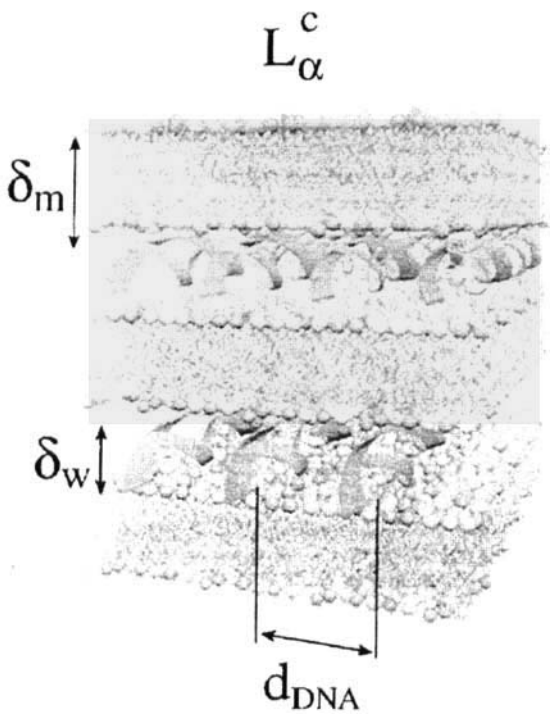

FIGURE 3 Schematic structure of the lamellar L_α^C phase of cationic lipid–DNA (CL–DNA) complexes showing alternating lipid bilayers and DNA monolayers. The interlayer spacing is $d = \delta_w + \delta_m$.

SAXS) is given by the simple geometric relation $d = \delta_m/(1 - \Phi_w)$. For membranes of pure DOTAP $\delta_m = 33 \pm 1$ Å (Raedler *et al.*, 1997). Highly dilute liposomes of DOTAP (with $\Phi_w \approx 98.5\%$ used in the SAXS experiments) do not exhibit Bragg diffraction in the small wave-vector range covered in Fig. 2. Thus, the DNA that condenses on the cationic membranes strongly screens the electrostatic interaction between lipid bilayers and leads to condensed multilayers. The average thickness of the water gap $\delta_w = d - \delta_m = 57$ Å $- 33$ Å $= 24$ Å ± 1 Å is just sufficient to accommodate one monolayer of B-DNA (diameter ≈ 20 Å) including a hydration shell (Podgornik *et al.*, 1994).

As we now discuss, the broad peak denoted $q_{DNA} = 0.256$ Å^{-1} arises from DNA–DNA correlations and gives $d_{DNA} = 2\pi/q_{DNA} = 24.55$ Å (Fig. 2, bottom). The precise nature of the packing structure of λ-DNA within the lipid layers can be elucidated by conducting a lipid dilution experiment in the isoelectric point regime of the complex (Raedler *et al.*, 1997; Salditt *et al.*, 1997; Koltover *et al.*, 1999). In these experiments, the total lipid (L = DOTAP + DOPC) is increased while the charge of the overall complex, given by the ratio of cationic DOTAP to DNA, is kept constant at the isoelectric point, DOTAP/DNA = 2.20. The SAXS scans in Fig. 2 (arrows point to the DNA peak) show that $d_{DNA} = 2\pi/q_{DNA}$ increases with lipid dilution from 24.55 to 57.1 Å as Φ_{DOPC} increases from 0 to 0.75 (or equivalently increasing L/D from 2.2 to 8.8). Figure 4A plots d and d_{DNA} as a function L/D. The most compressed interaxial spacing of ≈ 24.55 Å at $\Phi_{DOPC} = 0$ approaches the short-range repulsive hard-core interaction of the B-DNA rods containing a hydration layer (Podgornik *et al.*, 1994).

The observed behavior is depicted schematically in Fig. 4B showing that as we add neutral lipid (at the isoelectric point) and therefore expand the total cationic surface we expect the DNA chains to also expand and increase their interaxial spacing. The solid line in Fig. 4A is derived from the simple geometric packing relationship

$$d_{DNA} = (A_D/\delta_m)(\rho_D/\rho_L)(L/D) \qquad (1)$$

which equates the cationic charge density (due to the mixture $DOTAP^+$ and DOPC) with the anionic charge density (due to DNA^-) and is only valid at the isoelectric point where there is no excess lipid or DNA coexisting with the complex (Raedler *et al.*, 1997; Salditt *et al.*, 1997; Koltover *et al.*, 1999). Here, $\rho_D = 1.7$ (g/cc) and $\rho_L = 1.07$ (g/cc) denote the densities of DNA and lipid respectively, δ_m the membrane thickness, and A_D the DNA area. $A_D = \mathrm{Wt}(\lambda)/(\rho_D L(\lambda)) = 186$ Å^2, $\mathrm{Wt}(\lambda)$ = weight of λ-DNA $= 31.5 * 10^6/(6.022 * 10^{23})$ g and $L(\lambda)$ = contour length of λ-DNA $= 48\,502 * 3.4$ Å. The agreement between the packing relationship (solid line) with the data over the measured interaxial distance from 24.55 to 57.1 Å (Fig. 4A) is quite remarkable given the fact that there are no adjustable

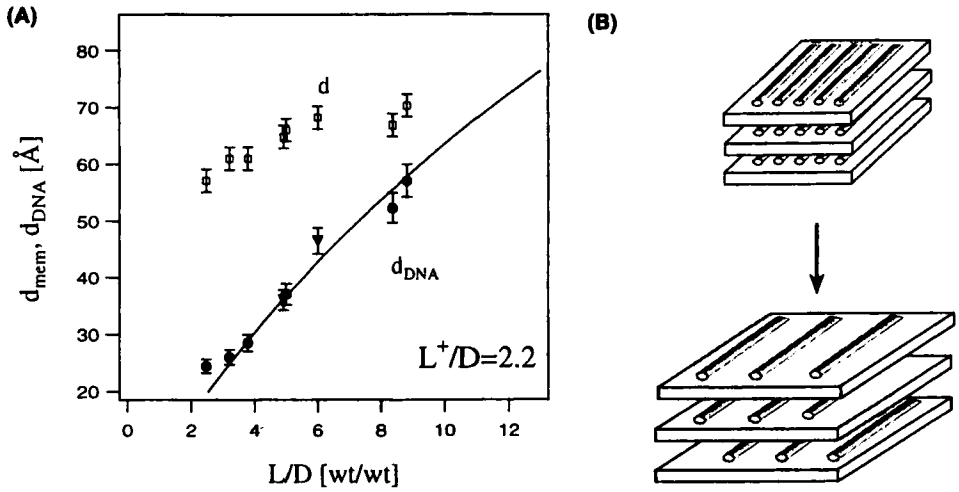

FIGURE 4 (A) The DNA interaxial distance d_{DNA} and the interlayer distance d in the L_α^C phase (Fig. 3) plotted as a function of Lipid/DNA (L/D) (wt./wt.) ratio at the isoelectric point of the complex, DOTAP/DNA = 2.2. d_{DNA} is seen to expand from 24.5 to 57.1 Å. The solid line through the data is the prediction of a packing calculation where the DNA chains form a space filling one-dimensional lattice. (Adapted from Raedler *et al.*, 1997; Salditt *et al.*, 1997; Koltover *et al.*, 1999). (B) Schematic drawing of DNA-membrane multilayers showing the increase in distance between DNA chains as the membrane charge density is decreased (i.e. as Φ_{DOPC} increases) at the isoelectric point.

parameters. The variation in the interlayer spacing $d(=\delta_w+\delta_m)$ (Fig. 4A, open squares) arises from the increase in the membrane bilayer thickness δ_m as L/D increases (each DOPC molecule is about 4–6 Å longer than a DOTAP molecule).

The observation of a *variation in the DNA interaxial distance* as a function of the lipid to DNA (L/D) ratio in multilayers (Fig. 4A) unambiguously demonstrates that XRD directly probes the DNA behavior in multilayer assemblies (Raedler *et al.*, 1997). From the linewidths of the DNA peaks, the 1D lattice of DNA chains is found to consist of domains extending to near 10 neighboring chains (Salditt *et al.*, 1997). Thus, the DNA chains form a finite-sized 1D ordered array adsorbed between 2D membranes; that is, a finite sized 2D smectic phase of matter (Raedler *et al.*, 1997; Salditt *et al.*, 1997; Koltover *et al.*, 1999).

The driving force for higher order self-assembly is the release of counterions. DNA carries 20 phosphate groups per helical pitch of 34.1 Å, and due to Manning condensation (Manning, 1969), 76% of these anionic groups are permanently neutralized by their counterions, which leads to a distance between anionic groups close to the Bjerrum length = 7.1 Å. During condensation, the cationic lipid tends to neutralize the phosphate groups on the DNA in effect replacing and releasing the originally condensed counterions (i.e. those bound to the 1D DNA and to the 2D cationic membranes) in solution.

3. METHODS AND MATERIALS

3.1. X-Ray and Optical Microscopy

X-Rays

Wide-angle and small-angle synchrotron X-ray scattering and diffraction were used for the quantitative *in situ* measurement of the self-assembled structures of CL–DNA complexes. X-rays diffracted by a sample with a periodic structure result in peak maxima at distinct q wave-vectors (related to the scattering angle). The ratio of the peak positions gives the lattice symmetry, revealing the specific structure of the sample (Warren, 1990). XRD experiments were carried out both with an in-house X-ray generator and at the Stanford Synchrotron Radiation Laboratory.

Optical Microscopy

Video-enhanced light microscopy techniques of phase, differential interference contrast (DIC) and reflection interference contrast, together with fluorescence microscopy (Nikon inverted, Diaphot 300) were used.

3.2. Materials and Sample Preparation

DNA

Both linear DNA (λ-phage, 48,502 bp) and two different functional supercoiled plasmids were used – pSV40-Luc (pGL3-control vector, Promega Corporation, Cat. #E1741) and pRSV-βgal.

Liposome Stock Solutions

Lipid components (DOTAP, DOPE, DOPC, Avanti Polar Lipids) were first dissolved in chloroform. To dissolve DOTAP completely we added 10% methanol to the chloroform solution. For labeled liposome samples, Texas Red® DHPE (Molecular Probes, Inc., Cat. #T-1395) was also dissolved in chloroform. The lipid solutions were mixed in required ratios in chloroform and methanol and allowed to evaporate, first under nitrogen, then in vacuum overnight, leaving a lipid film behind. Water was added to the dried lipid film and incubated for at least 6 h to allow formation of liposomes. Before making complexes, liposome solutions were vortexed for 1 min, tip-sonicated for 5–10 min, and filtered with 0.2 μm filters. An alternative method was to bath-sonicate for 2 h after vortexing. The liposome and CL–DNA complex sizes were measured by dynamic light scattering (Microtrac UPA 150, Leeds and Northrup).

Animal Cell Lines

Mouse fibroblast L-cell line was grown in DMEM(+/+) in an incubator set at 37°C and 5% CO_2 atmosphere. DMEM(+/+) is composed of DMEM (Dulbecco's Modified Eagles's Medium from Gibco BRL, Cat. #21063-029) supplemented with 1% penicillin–streptomycin (Gibco BRL, Cat. #15140-122) and 5% FBS (Fetal Bovine Serum from HyClone Laboratories, Inc., Cat. #SH30070.02). Cells were split every 2–4 days to maintain a monolayer coverage in culture flasks. Cells were washed once with 1 × PBS (diluted from Gibco BRL, Cat. #70013-032) before adding trypsin (Gibco BRL, Cat. #25300-054) to detach the cells from the bottom of culture flasks. We then mixed the detached cells in DMEM(+/+) and seeded an appropriate portion for growth.

To Prepare X-ray Samples of Complexes in DMEM or DMEM(+/+)

Equal volumes of DMEM or DMEM(+/+) were added to DNA and lipid stock solutions in water. The resulting solutions were loaded into X-ray capillaries by first centrifuging down the lipid solution, followed by the DNA solution, and finally centrifuging the mixture at 9000 rpm for 15–30 min.

Fluorescent Labels for Lipid and DNA

Preparation for DIC and Fluorescence Optical Microscopy Studies of Transfected Cells 22 mm × 22 mm coverslips were sonicated in detergent for half an hour, rinsed 10 times with deionized water, and baked in a 185°F oven for 2 h before use. L-cells were seeded on the coverslips in 6-well plates and allowed to grow for 20 h before experiments so that the confluency reached 60–80% at the time of transfection. We prepared complexes fresh each time immediately before transfection. The DNA in the complexes was labeled with YOYO®-1 (Molecular Probes, Cat. #Y-3601, 491/509 green) and the lipid was labeled with Texas Red® DHPE. For covalent attachment to DNA we used Mirus Label IT™ Nucleic Acid Labeling Kits (from PanVera Corp., fluorescein-green 494/518 and rhodamine-red 570/590) which allows the marker to attach within 1 h. Other DNA and lipid labels included YOYO®-3 (612/631 red) for DNA and TRITC-DHPE (540/566, yellow-green), and fluorescein-DHPE (496/519, green) for lipid. The dyed DNA and lipid stocks were diluted in DMEM separately

to make a final volume of 500 µl each. The diluted solutions were mixed together and left for 20 min to allow formation of complexes. To transfect, cells were washed once in 1× PBS and incubated in complex solutions at 37°C for various lengths of time. The complex solutions were then removed, after which the cells were washed three times with 1× PBS and fixed by soaking in fixing solution (0.1% glutaldehyde and 4% formaldehyde in 1× PBS) for 20–30 min. We removed the fixing solution before mounting the coverslips for observation under the microscope (Nikon inverted, Diaphot 300, or BioRad 1024 confocal at the Neuroscience Research Institute). Each coverslip was soaked in seven or eight drops of equilibration buffer from the SlowFade® Light Antifade Kit (Molecular Probes, Inc. Cat. #S-7461) for 5–10 min, then mounted on a 24 × 60 mm microslide with one drop (8 µl) of SlowFade® mounting medium (also from the kit). Finally, the samples were sealed with regular red nail polish and may be stored for at least two weeks at 4°C.

Luciferase Assays of pGL3 DNA

To prepare samples for assays, L-cells were directly plated in a 6-well, 24-well, or 96-well plate 20 h before transfection so that the confluency reached 60–80% at the time of transfection. Complexes were prepared just prior to being laid on cells. First, DNA stock and lipid stock were diluted in DMEM separately to make a final volume of 500 µl each. They were then mixed together and left for 20 min to allow formation of complexes. Cells in plates were washed once in 1× PBS before complex solutions were added. The plates were then incubated at 37°C in 5% CO_2 atmosphere for 6 h. After 6 h, complex solutions were removed and the cells were washed three times with 1× PBS before DMEM(+/+) was added. The plates were then incubated for an additional 24 h to allow the expression of the transgene.

The transfected cells were washed once with 1× PBS. Then an appropriate amount of Luciferase Cell Lysis Reagent (Progema Corp. Cat. #E1531) was applied to the cells (300 µl for 35 mm wells; 150 µl for 15 mm wells). The cells were then placed on ice for 5 min and then scraped off the bottom of the well. The resulting solution was stored at −20°C. The readings for luciferase activity were done on a Optocomp I Luminometer (MGM Instruments, Inc.). Twenty µl of room temperature cell extract were mixed with 100 µl of room temperature Luciferase Assay Reagent (Promega Corp. Cat. #E1501). This mixture was placed in the luminometer where the reading of the number of photons emitted, expressed in relative light units (RLU), was integrated over a 20 s time period. Two readings were taken for each sample and then averaged. To convert RLU to actual amount of protein, a standard was run using recombinant luciferase (Promega Corp. Cat. #E1701).

4. RESULTS

It is known that transfection efficiency mediated by mixtures of cationic lipids and neutral "helper-lipids" varies widely and unpredictably (Zhu *et al.*, 1993; Nabel *et al.*, 1993; Mulligan, 1993; Felgner and Rhodes, 1991; Behr, 1994; Remy *et al.*, 1994; Singhal and Huang, 1994; Lasic and Templeton, 1996). The choice of the helper-lipid has been empirically established to be important (Remy *et al.*, 1994; Felgner *et al.*, 1994; Farhood *et al.*, 1995; Hui *et al.*, 1996); for example, many papers report that transfection is believed to be efficient in mixtures of the cationic lipid DOTAP and the neutral helper-lipid DOPE, and not in mixtures of DOTAP and the similar helper-lipid DOPC. For the moment, we concentrate on the univalent cationic lipid system DOTAP where we have X-ray data on the structure in a similar concentration range as the transfection results. Figure 5 shows our transfection results for DOTAP/DOPC ($\Phi_{DOPC} = 0.72$) and DOTAP/DOPE ($\Phi_{DOPE} = 0.72$) containing complexes as a function of DOTAP/DNA for negative (below dashed line) and positive (above dashed line) complexes. We see that at these composition the DOPE containing complexes are significantly more transfectant.

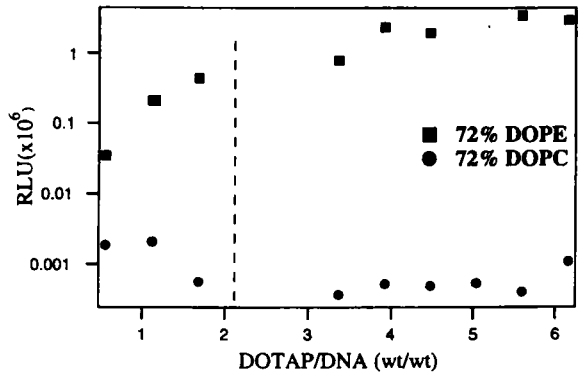

FIGURE 5 Luciferase reporter gene (pGL3-control vector) activity measured in transfected fibroblast L-cells. Transfection efficiencies for positive (DOTAP/DNA > 2.2) and negative (DOTAP/DNA < 2.2) CL–DNA complexes are shown. The squares are for DOPE/DOTAP CLs (72% DOPE), the circles are for DOPC/DOTAP CLs (72% DOPC). Transfections were done in 24-well plates with 2 μg of DNA and varying amounts of lipid. 10^6 RLU (relative light units) corresponds to 0.025 ng of luciferase. Background (instrument noise level) done with a control containing no complex is 10 RLU.

Our recent SAXS data shows that in the similar concentration regime the biologically active pGL3 luciferase supercoiled plasmid complexed with DOTAP/DOPC suspended in DMEM (cell medium during transfer of complexes as described in the methods section) exhibit the lamellar L_α^C structure (Fig. 7, left), analogous to the structure in DOPC/DOTAP–λ-DNA complexes. At $\Phi_{DOPC} = 0.72$, SAXS of the lamellar L_α^C complex shows sharp peaks at $q_{001} = 0.088\,\text{Å}^{-1}$, $q_{002} = 0.176\,\text{Å}^{-1}$, $q_{003} = 0.264\,\text{Å}^{-1}$, and $q_{004} = 0.352\,\text{Å}^{-1}$, resulting from the lamellar periodic structure ($d = 2\pi/q_{001} = 71.40$ Å) with plasmid–DNA intercalated between cationic lipid bilayers. Our SAXS data shows that in fact DOPE containing complexes may give rise to a completely different self-assembled structure. For $\Phi_{DOPE} = 0.72$ (Fig. 7, right), the peaks of the SAXS scans of the CL–DNA complexes are indexed perfectly on a two-dimensional (2D) hexagonal lattice with a unit cell spacing of $a = 4\pi/((3)^{0.5} q_{10}) = 69.10$ Å. The SAXS data shows the first seven order Bragg peaks of this hexagonal structure at $q_{10} = 0.105\,\text{Å}^{-1}$, $q_{11} = 0.182\,\text{Å}^{-1}$, $q_{20} = 0.21\,\text{Å}^{-1}$, $q_{21} = 0.273\,\text{Å}^{-1}$, $q_{30} = 0.31\,\text{Å}^{-1}$, $q_{22} = 0.364\,\text{Å}^{-1}$, $q_{32} = 0.46\,\text{Å}^{-1}$. The structure is consistent with a 2D columnar inverted hexagonal structure (Fig. 8) which we refer to as the H_{II}^C phase of CL–DNA complexes. The DNA molecules are surrounded by a lipid monolayer with the DNA/lipid inverted cylindrical micelles arranged on a hexagonal lattice. The H_{II}^C structure was originally observed in DOPE containing CL–DNA complexes with linear λ-DNA (Koltover *et al.*, 1998).

To understand the stability of the lamellar and hexagonal phases we consider the interplay between the electrostatic and membrane elastic interactions in the CL–DNA complexes which is expected to determine the different structures. Recent theoretical work suggests that electrostatic interactions alone are expected to favor the inverted hexagonal H_{II}^C phase (Fig. 8) over the lamellar L_α^C, due to the natural tendency to minimize the charge separation between the anionic groups on the DNA chain and the cationic lipids (May and Ben-Shaul, 1997; Dan, 1998). However, the electrostatic interaction may be resisted by the membrane elastic cost (per unit area) (Seddon, 1989; Gruner, 1989; Israelachvili, 1992; Janiak *et al.*, 1979) of forming a cylindrical monolayer membrane around DNA

$$F/A = 0.5\kappa(1/R - 1/R_0)^2 \qquad (2)$$

Here, κ is the lipid monolayer bending rigidity, R the actual radius and R_0 the natural radius of curvature of the monolayer. Figure 6 shows schematically the possible "shapes" of many common lipids. For example, many lipids (e.g. phosphatidylcholine, phosphotidylserine, phosphotidylglycerol, cardiolipin) have a cylindrical shape, with the head group area ≈ the hydrophobic tail area, and tend to self-assemble into lamellar structures with a natural curvature $C_0 = 1/R_0 = 0$. Other lipids (e.g. phosphotidylethanolamine) have a cone shape, with a smaller head group area than tail area, and give rise to a negative natural curvature $C_0 < 0$. Alternatively, lipids with a larger head group than tail area have $C_0 > 0$.

It is well appreciated (Seddon, 1989; Gruner, 1989; Israelachvili, 1992; Janiak *et al.*, 1979) that in many lipid systems the "shape" of the molecule

which determines the natural curvature of the membrane $C_0 = 1/R_0$ will also determine the actual curvature $C = 1/R$ that describes the structure of the lipid self-assembly (e.g. $C = 0 \rightarrow$ lamellar L_α; $C_0 < 0 \rightarrow$ inverted hexagonal H_{II}; $C_0 > 0 \rightarrow$ hexagonal H_I). This is particularly true if the bending rigidity of the membrane is large ($\kappa/k_BT \gg 1$), because then a significant deviation of C from C_0 would cost too much elastic energy. We can understand the L_α^C to H_{II}^C transition as a function of increasing Φ_{DOPE} (Koltover *et al.*, 1998) by noting that in contrast to the helper-lipid DOPC and the cationic lipid DOTAP which have a zero natural curvature ($C_0^{DOTAP,DOPC} = 1/R_0^{DOTAP,DOPC} = 0$), DOPE is cone-shaped with $C_0^{DOPE} = 1/R_0^{DOPE} < 0$ (Fig. 6). Consequently, the natural curvature of the monolayer mixture of DOTAP and DOPE is driven negative with $C_0 = 1/R_0 = \Phi_{DOPE} C_0^{DOPE}$. It follows that as a function of increasing Φ_{DOPE} we expect a transition from the L_α^C to the H_{II}^C phase which is observed experimentally and is now also expected to be favored by the elastic free energy. Thus, the helper-lipid DOPE induces the L_α^C to H_{II}^C transition by controlling the spontaneous radius of curvature R_0 of the lipid layers.

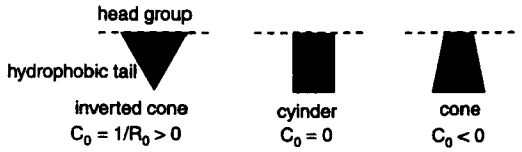

FIGURE 6 Three possible shapes of common lipid molecules as described in the text.

The importance of the precise self-assembled structures to biological function is underscored in preliminary optical imaging experiments described below which show that interactions of CL–DNA complexes with mouse fibroblast cells are structure-dependent (e.g. H_{II}^C versus L_α^C). Current data from several laboratories (Zabner *et al.*, 1995; Wrobel and Collins, 1995; Xu and Szoka, 1996) indicates that one of the main entry routes of complexes is endocytosis following attachment of the positive CL–DNA complexes to negatively charged cell surface proteoglycans (Mislick and Baldeschwieler,

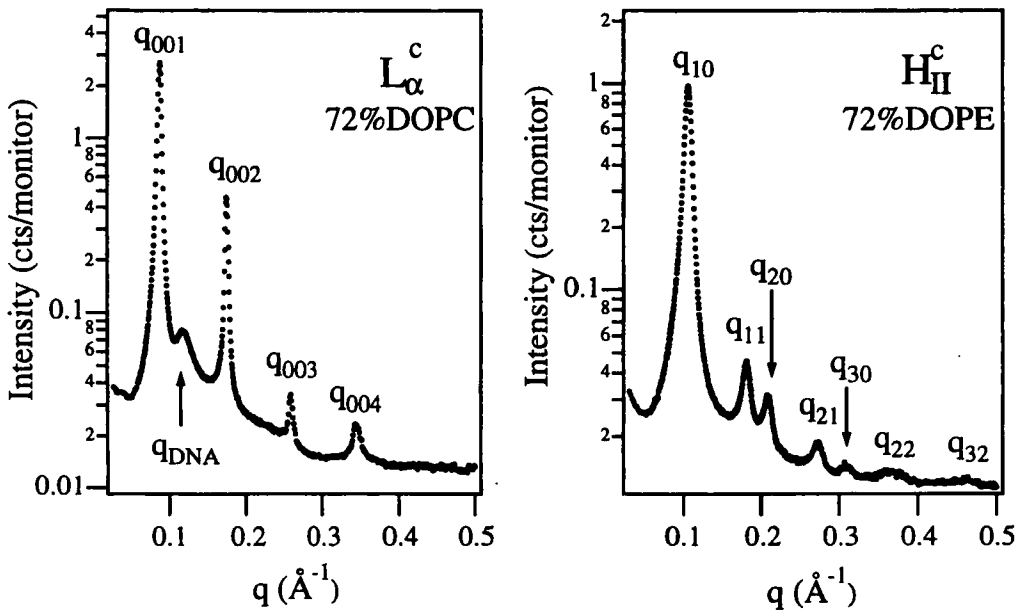

FIGURE 7 XRD data of positive complexes (DOTAP/plasmid = 4) containing pGL3 luciferase plasmid and DOTAP mixed with helper-lipid in DMEM. (Left) shows a lamellar structure at 72% DOPC, with $d = 71.40$ Å. (Right) shows an inverted hexagonal structure at 72% DOPE, with $a = 69.10$ Å.

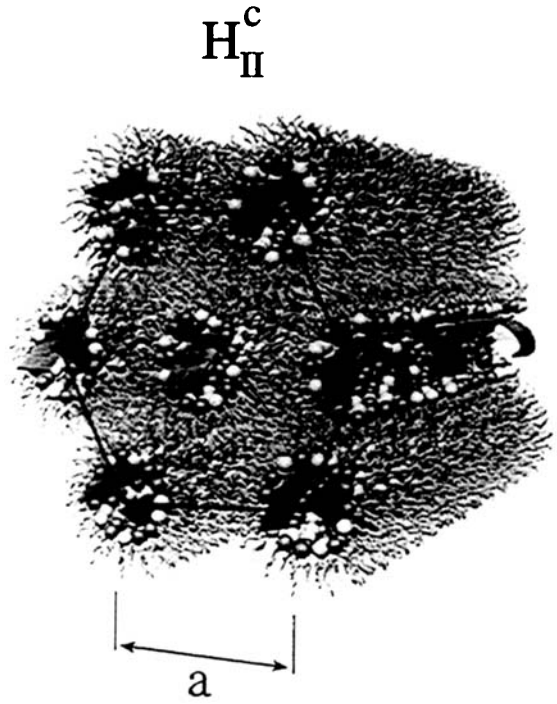

FIGURE 8 Schematic of the inverted hexagonal H_{II}^{C} phase (cylinders consisting of DNA coated with a lipid monolayer arranged on a hexagonal lattice) of cationic lipid–DNA (CL–DNA) complexes.

1996). Thus, at the very early stages of cell transfection, an intact CL–DNA complex is captured inside an endosome which contains anionic lipids.

To date, there are few optical imaging data on CL–DNA complexes inside cells. Biochemical functional data on transfection efficiency cannot independently elucidate the molecular and self-assembled mechanisms involved in the transfer of the complex to the nuclear region. Direct imaging *in vitro* should allow us to elucidate the various pathways between the plasma membrane and the nucleus. We show in Figs. 9 and 10 optical micrographs of transfected cells, representative of the behaviors of over 80% of the cell population. Figure 9 shows results where L_{α}^{C} CL–DNA complexes have been allowed to interact with mouse fibroblasts cells for 1 h followed by fixing of the transfected cells in preparation for observations. Fluorescence labeling of both lipid and DNA allows us to determine their exact locations relative to the cells. Left (Fig. 9) shows optical micrographs of the cells in DIC. The complexes inside the cell are identified by simultaneously observing the green

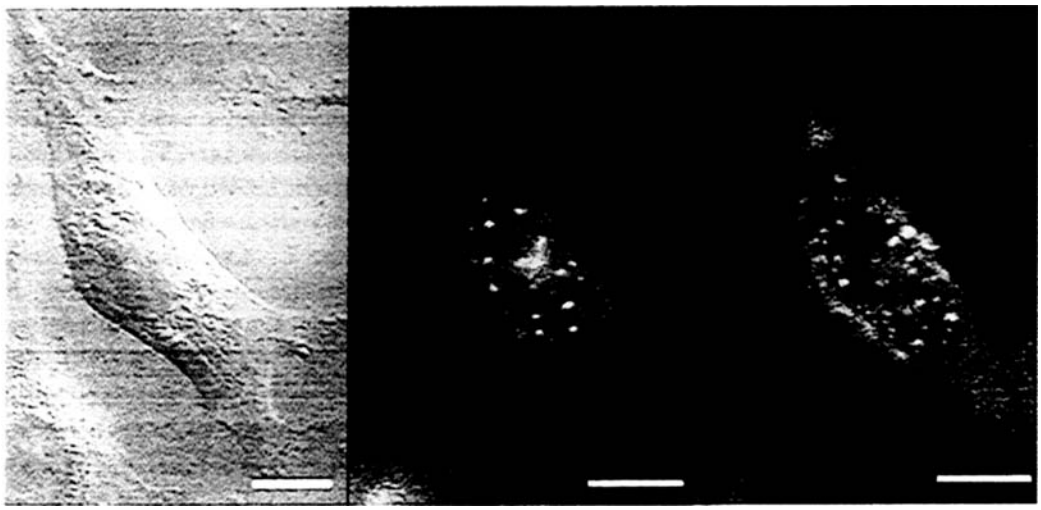

FIGURE 9 Images of mouse fibroblast L-cells mixed with positively charged (L/D = 10) CL–DNA complexes with the L_{α}^{C} structure (50% DOPC–50% DOTAP–βgal DNA) and fixed 1 h after the transfection experiment. DIC image (left) of transfected cell attached to glass. The position of the complexes are visualized inside the cells through double-fluorescence which shows both the YOYO-DNA green fluorescence (center) and the Texas-Red-DHPE (lipid tag) (right). Matching dots imply a complex (e.g. circles in right). Bar is 10 μm.

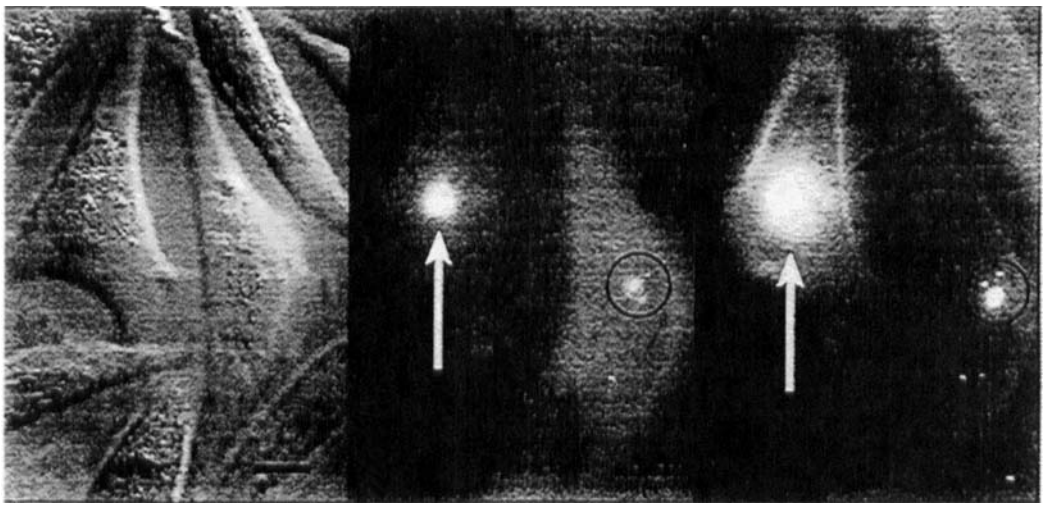

FIGURE 10 Images of mouse fibroblast L-cells mixed with positively charged (L/D = 10) CL–DNA complexes with the H_{II}^C structure (50% DOPE–50% DOTAP–βgal DNA) and fixed 1 h after the transfection experiment. DIC image of transfected cells (left) attached to glass. YOYO-DNA green fluorescence mode is shown in the center and the Texas-Red-DHPE (lipid tag) on the right. The lipid is seen to have fused with the plasma membrane (right, black arrow). The white arrows (center and right) show the presence of aggregated clusters of CL–DNA complexes. A few isolated complexes are also seen (black circles). Bar is 10 μm.

fluorescence of YOYO-DNA (center, Fig. 9) and the red fluorescence of Texas Red-DHPE (right, Fig. 9). Despite the fuzziness in the images caused by diffused scattering from out-of-focus planes, the separated dots indicating small aggregates of lipid and DNA can be distinctly observed. The presence of numerous complexes where the two dyes coincide spatially is clearly evident.

Figure 10 displays optical micrographs similar to Fig. 9 but now with H_{II}^C CL–DNA complexes incorporating DOPE helper-lipid. The behavior with H_{II}^C complexes is clearly different where we now observe fusion of lipid with the cell plasma membrane (right, black arrow) indicated by the sharply focused outline of the plasma membrane in the lipid fluorescent mode. Following endocytosis, the H_{II}^C self-assembly enters the cell inside an anionic endosomal vesicle. It may then fuse with the endosomal membrane either completely or partially and release DNA into the cytosol. Released lipid from the CL–DNA (both cationic and helper-lipid) would be expected to mix with the plasma membrane (which acts like a large reservoir for free lipid) producing the fused image (Fig. 10, right). We see evidence of aggregation of CL–DNA complexes (Fig. 10, white arrows) and also some intact complexes (Fig. 10, black circles).

5. DISCUSSION

The data represent one example of a correlation between the self-assembled structure of CL–DNA complexes and transfection efficiency for this particular concentration regime in DOTAP/DOPE and DOTAP/DOPC complexes. The empirically established transfectant DOPE containing complexes in mammalian cell cultures exhibit the H_{II}^C structure rather than the L_α^C found in DOPC containing complexes. Further, optical microscopy reveals a most likely origin for why the different structures transfect cells with varying efficiency: in contrast to L_α^C complexes which remain stable inside cells (Fig. 9), H_{II}^C complexes show fusion of their lipid with the mouse cell membranes (e.g. endosomal and plasma membranes) (Fig. 10) which results in DNA release.

A major motivation for elucidating the structures and interactions in these CL–DNA complexes arises because they are promising synthetic nonviral

gene delivery systems. Cationic liposome transfer vectors exhibit low toxicity, nonimmunogenicity, and ease of production, but their mechanism of action remains largely unknown with transfection efficiencies varying by up to a factor of 100 in different cell lines. This unpredictability, which is ubiquitous in gene therapy (Felgner, 1997; Miller, 1998; Crystal, 1995; Felgner *et al.*, 1987) and in particular in synthetic systems, may in part be attributed to a lack of knowledge regarding the interactions between DNA and CLs, the resulting structures of CL–DNA complexes, and in turn, their interactions with cells at the molecular and self-assembled levels.

In the long run, we expect that a more complete set of structure–function data should allow us to begin the formidable task of a rational design of these self-assemblies for enhanced gene delivery applications from the ground up beginning with the chemical structure of the lipids and the optimal compositions in mixtures including functional plasmid.

There are currently two main routes of gene delivery into the human body. The more common method, *ex vivo*, refers to removing cells from a patient, delivering foreign genes in the laboratory, and returning the altered cells to the body. The other is the *in vivo* method where genes are directly introduced into the body. Clinical trials have been initiated using the cationic lipid delivery systems (Felgner, 1997; Miller, 1998), showing limited success in the intratumoral injection of plasmid DNA mixed with DMRIE/DOPE (Stopeck *et al.*, 1998; Clark *et al.*, 1999). Our research in understanding the mechanisms of gene uptake and expression in cells will directly aid in optimizing the *ex vivo* method, as well as help us elucidate how genes will interact with the cells once injected into the body.

Finally, aside from the medical and biotechnological ramifications in gene therapy and gene and drug therapeutics, the research should also shed light on other problems in biology. The development of efficient HAC vectors in the future, which will most likely occur once efficient synthetic nonviral delivery systems have been developed, is a long range goal in studies designed to characterize chromosome structure and function.

Acknowledgments

Supported by National Institutes of Health Research Grants R01 GM59288-01 and R37 AI12520-24, and University of California Biotechnology Research and Education Program Training Grant 97-02. The synchrotron X-ray experiments were carried out at the Stanford Synchrotron Radiation Laboratory which is supported by the US DOE. The Materials Research Laboratory at Santa Barbara is supported by NSF-DMR-9632716.

References

Behr, J.P. (1994) Gene transfers with synthetic cationic amphiphiles-prospects for gene therapy. *Biconjugate Chem.* **5**, 382–389.

Brigham, K.L., Meyrick, B., Christman, B., Magnuson, M., King, G. and Berry, L.C. (1989) *In vivo* transfection of murine lungs with a functioning prokaryotic gene using a liposome vehicle. *Am. J. Med. Sci.* **298**, 278–281.

Clark, P.R., Stopeck, A.T., Brailey, J.L., Wang, Q., McArthur, J., Finer, M.H. and Hersh, E.M. (1999) Polycations and cationic lipids enhance adenovirus transduction and transgene expression in tumor cells. *Cancer Gene Therapy* **6**, 437–446.

Crystal, R.G. (1995) Transfer of genes to humans-early lessons and obstacles to success. *Science* **270**, 404–410.

Dan, N. (1998) The structure of DNA complexes with cationic liposomes – cylindrical or flat bilayers? *Biochim. Biophys. Acta* **1369**, 34–38.

Farhood, H., Serbina, N. and Huang, L. (1995) The role of dioleoyl phospatidylethanolamine in cationic liposome mediated gene therapy. *Biochim. Biophys. Acta – Biomembranes* **1235**, 289–295.

Felgner, J.H., Kumar, R., Sridhar, C.N., Wheeler, C.J., Tsai, Y.J., Border, R., Ramsey, P., Martin, M. and Felgner, P.L. (1994) Enhanced gene delivery and mechanism studies with a novel series of cationic lipid formulations. *J. Biol. Chem.* **269**, 2550–2561.

Felgner, P.L. (1997) Nonviral strategies for gene therapy. *Sci. Am.* **276**, 102–106.

Felgner, P.L., Gadek, T.R., Holm, M., Roman, R., Chan, H.W., Wenz, M., Northrop, J.P., Ringold, G.M. and Danielsen, M. (1987) Lipofection: A highly efficient, lipid-mediated DNA-transfection procedure. *Proc. Nat. Acad. Sci. USA* **84**, 7413–7417.

Felgner, P.L. and Rhodes, G. (1991) Gene therapeutics. *Nature* **349**, 351–352.

Friedmann, T. (1997) Overcoming obstacles to gene therapy. *Sci. Am.* **276**, 96–101.

Gershon, H., Ghirlando, R., Guttmann, S.B. and Minsky, A. (1993) Mode of formation and structural features of DNA cationic liposome complexes used for transfection. *Biochem.* **32**, 7143–7151.

Gruner, S.M. (1989) Stability of lyotropic phases with curved interfaces. *J. Phys. Chem.* **93**, 7562–7570.

Gustafsson, J., Arvidson, G., Karlsson, G. and Almgren, M. (1995) Complexes between cationic liposomes and DNA visualized by cryo-TEM. *Biochim. Biophys. Acta* **1235**, 305–312.

Harrington, J.J., Van Bokkelen, G., Mays, R.W., Gustashaw, K. and Williard, H.F. (1997) Formation of *de novo* centromeres and construction of first-generation human artificial microchromosomes. *Nature Gen.* **15**, 345–355.

Hazinski, T.A., Ladd, P.A. and Dematteo, C.A. (1991) Localization and induced expression of fusion genes in the rat lung. *Am. J. Resp. Cell Mol. Bio.* **4**, 206–209.

Helfrich, W. (1978) Steric interaction of fluid membranes in multilayer systems. *Zeitschift fur Naturforschung A* **33**, 305–315.

Holt, C.E., Garlick, N. and Cornel, E. (1990) Lipofection of cDNAs in the embryonic vertebrate central nervous system. *Neuron* **4**, 203–214.

Hui, S.W., Langner, M., Zhao, Y.L. and Ross, P. *et al.* (1996) The role of helper lipids in cationic liposome-mediated gene transfer. *Biophys. J.* **71**, 590–599.

Israelachvili, J.N. (1992) *Intermolecular and Surface Forces.* 2nd edn. (Academic Press, London).

Janiak, M.J., Small, D.M. and Shipley, G.G. (1979) Temperature and compositional dependence of the structure of hydrated dimyristoyl lecithin. *J. Biol. Chem.* **254**, 6068–6078.

Koltover, I., Salditt, T., Raedler, J.O. and Safinya, C.R. (1998) An inverted hexagonal phase of DNA–cationic liposome complexes related to DNA release and delivery *Science* **281**, 78–81.

Koltover, I., Salditt, T. and Safinya, C.R. (1999) Phase diagram, stability and overcharging of lamellar cationic lipid–DNA self-assembled complexes. *Biophys. J.* **77**(2), 915–924.

Lasic, D. and Templeton, N.S. (1996) Liposomes in gene therapy. *Adv. Drug Del. Rev.* **20**, 221–266.

Lasic, D.D., Strey, H.H., Stuart, M.C.A., Podgornik, R. and Frederik, P.M. (1997) The structure of DNA–liposome complexes. *J. Am. Chem. Soc.* **119**, 832–833.

Malone, R.W. (1989) Expression of chloramphenicol acetyltransferase activity in brain tissue of frog embryos with cationic liposome vectors. *Focus* **11**, 4.

Manning, G.S. (1969) Limiting laws and counterion condensation in polyelectrolyte solutions. I. Colligative properties. *J. Chem. Phys.* **51**, 924–933.

Marshall, E. (1995) Gene therapy's growing pains. *Science* **269**, 1050–1055.

May, S. and Ben-Shaul, A. (1997) DNA–lipid complexes: stability of honeycomb-like and spaghetti-like structures. *Biophys. J.* **73**, 2427–2440.

Miller, A.D. (1998) Cationic liposomes for gene therapy. *Ang. Chem. (International Edition), Rev.* **37**, 1768–1785.

Mislick, K.A. and Baldeschwieler, J.D. (1996) Evidence for the role of proteoglycans in cation mediated gene transfer. *Proc. Nat. Acad. Sci. USA* **93**, 12 349–12 354.

Mulligan, R.C. (1993) The basic science of gene therapy. *Science* **260**, 926–932.

Nabel, G.J., Nabel, E.G., Yang, Z.Y., Fox, B.A., Plautz, G.E., Gao, X., Huang, L., Shu, S., Gordon, D. and Chang, A.E. (1993) Direct gene transfer with DNA liposome complexes in melanoma-expression, biologic activity, and lack of toxicity in humans. *Proc. Nat. Acad. Sci. USA*, **90**, 11 307–11 311.

Ono, T., Fujino, Y., Tsuchiya, T. and Tsuda, M. (1990) Plasmid DNAs directly injected into mouse brain with lipofection can be incorporated and expressed by brain cells. *Neurosci. Lett.* **117**, 259–263.

Pitard, B., Aguerre, O., Airiau, M., Lachagès, A.-M., Boukhnikachvili, T., Byk, G., Dubertret, C., Herviou, C., Scherman, D., Mayaux, J.-F. and Crouzet, J. (1997) Virus sized self-assembled lamellar complexes between plasmid DNA and cationic micelles promote gene transfer. *Proc. Natl. Acad. Sci. USA* 94, 14 412–14 417.

Podgornik, R., Rau, D.C. and Parsegian, V.A. (1994) Parametrization of direct and soft steric-undulatory forces between DNA double helical polyelectrolytes in solutions of several different anions and cations. *Biophys. J.* **66**, 962–971.

Raedler, J.O., Koltover, I., Salditt, T. and Safinya, C.R. (1997) Structure of DNA–cationic liposome complexes: DNA intercalation in multi-lamellar membranes in distinct interhelical packing regimes. *Science* **275**, 810–814.

Raedler, J.O., Koltover, I., Salditt, T., Jamieson, A. and Safinya, C.R. (1998) Structure and interfacial aspects of self-assembled cationic lipid–DNA gene carrier complexes. *Langmuir* **14**, 4272–4283.

Remy, J.S., Sirlin, C., Vierling, P. and Behr, J.P. (1994) Gene transfer with a series of lipophilic DNA-binding molecules. *Biconjugate Chem.* **5**, 647–654.

Roush, W. (1997) Molecular biology-counterfeit chromosomes for humans. *Science* **276**, 38–39.

Roux, D. and Safinya, C.R. (1988) A synchroton X-ray study of competing undulation and electrostatic interlayer interactions in fluid multimembrane lyotropic phases. *J. Physique France* **49**, 307–318.

Salditt, T., Koltover, I., Raedler, J.O. and Safinya, C.R. (1997) Two-dimensional smectic ordering of linear DNA chains in self-assembled DNA–cationic liposome mixture. *Phys. Rev. Lett.* **79**, 2582–2585.

Salditt, T., Koltover, I., Raedler, J.O. and Safinya, C.R. (1998) Self-assembled DNA–cationic lipid complexes: two-dimensional smectic ordering, correlations, and interactions. *Phys. Rev. E* **58**, 889–904.

Safinya, C.R. (1989) Rigid and fluctuating surfaces: a series of synchrotron X-ray scattering studies of interacting stacked membranes. In Tormod, R. and Sherrington, D. (Eds.), *Phase Transitions in Soft Condensed Matter* (Plenum, New York), pp. 249–270.

Safinya, C.R. and Koltover, I. (1999) Self assembled structures of lipid–DNA nonviral gene delivery systems from synchrotron X-ray diffraction. In Huang, L., Hung, M.C. and Wagner E. (Eds.), *Non-Viral Vectors For Gene Therapy* (Academic Press, San Diego), pp. 91–117.

Safinya, C.R., Koltover, I. and Raedler, J.O. (1998) DNA at membrane surfaces: an experimental overview. *Curr. Opin. Colloid Interface Sci.* **3**(1), 69.

Seddon, J.M. (1989) Structure of the inverted hexagonal phase and non-lamellar phase transitions of lipids. *Biochim. Biophys. Acta* **1031**, 1–69.

Singhal, A. and Huang, L. (1994) Gene transfer in mammalian cells using liposomes as carriers. In Wolff, J.A. (Ed.), *Gene Therapeutics: Methods and Applications of Direct Gene Transfer* (Birkhauser, Boston), pp. 110–120.

Sternberg, B., Sorgi, F.L. and Huang, L. (1994) New structures in complex formation between DNA and cationic liposomes visualized by freeze-fracture electron microscopy. *FEBS Lett.* **356**, 361–366.

Stopeck, A.T., Hersh, E.M., Brailey, J.L., Norman, J. and Parker, S.E. (1998) Transfection of primary tumor cells and

tumor cell lines with plasmid DNA/lipid complexes. *Cancer Gene Therapy* **5**, 119–126.
Stribling, R., Brunette, E., Liggitt, D., Gaensler, K. and Debs, R. (1992) Aerosol gene delivery *in vivo*. *Proc. Natl. Acad. Sci. USA* **89**, 11 277–11 281.
Warren, B.E. (1990) *X-Ray Diffraction*. (Dover Publications, Inc., New York).
Wrobel, I. and Collins, D. (1995) Fusion of cationic liposomes with mammalian cells occurs after endocytosis. *Biochim. Biophys. Acta* – Biomembranes **1235**, 296–304.
Xu, Y. and Szoka, F.C. (1996) Mechanism of DNA release from cationic liposome/DNA complexes used in cell transfection. *Biochem.* **35**, 5616–5623.
Zabner, J., Fasbender, A.J., Moninger, T., Poelinger, K.A. and Welsh, M.J. (1995) Cellular and molecular barriers to gene transfer by a cationic lipid. *J. Biol. Chem.* **270**, 18 997–19 007.
Zhu, N., Liggitt, D., Liu, Y. and Debs, R. (1993) Systemic gene expression after intravenous DNA delivery into adult mice. *Science* **261**, 209–211.